Large magnetoresistance and quantum oscillations of a ternary boride MoAlB single crystal

Lingxiao Zhao,* Liangcai Xu, Linchao Ding, Huakun Zuo, and Zengwei Zhu†
Wuhan National High Magnetic Field Center, School of Physics, Huazhong University of Science and Technology, Wuhan 430074, China

(Received 9 March 2020; revised 17 July 2020; accepted 6 August 2020; published 26 August 2020)

We report transport properties in a ternary compound MoAlB single crystal. It shows a metallic behavior with a residual resistivity ratio of $\rho(300\ \mathrm{K})/\rho(2\ \mathrm{K})$=40. After applied magnetic fields, the resistivity shows a quick upturn and saturates to a plateau as the temperature decreasing. At 2 K, the magnetoresistance (MR) increases quadratically with the magnetic field and reaches up to 1650% ($B = 14$ T) without saturation. The two-band fitting of the Hall conductivity suggests that the unsaturated large quadratic MR in MoAlB was originated from the carriers' compensation with high mobility ($\mu_h = 7104\ \mathrm{cm^2\,V^{-1}\,s^{-1}}$ and $\mu_e = 1432\ \mathrm{cm^2\,V^{-1}\,s^{-1}}$). The angle dependence of the ρ_{xx} shows significant anisotropy. Furthermore, pronounced Shubnikov-de Haas (SdH) oscillations are observed in both magnetoresistivity and Hall resistivity. We analyzed these quantum oscillations carefully and revealed several small Fermi surfaces with the light cyclotron masses in MoAlB. The angle dependence of SdH oscillations reveals quasi-two-dimensional Fermi surface structure in MoAlB.

DOI: 10.1103/PhysRevB.102.075139

I. INTRODUCTION

Since the discovery of the extremely large magnetoresistance (XMR) property in the nonmagnetic material WTe_2 [1], researching materials with large magnetoresistance has attracted tremendous attention. Until now, a series of XMR materials have been discovered and three main convincing mechanisms have been suggested to explain the XMR effect in those nonmagnetic semimetals. The first one is the electron-hole compensation mechanism. In semimetals with similar densities of electrons and holes, the magnetoresistance (MR) can be written as $\mathrm{MR} = \mu_e\mu_h B^2$, where μ_e and μ_h is the mobility of the electrons and holes, respectively. In these materials, the MR increases quadratically with the strength of magnetic field B. The XMR materials such as WTe_2, α-As, $PtBi_2$, $TaAs_2$, $NbSb_2$, and YSb [1–8] were found to be good compensated semimetals with MR over 10^5%. The second explanation is the topological protection. In topological materials, the backscattering is suppressed by the topological protection without magnetic field. The lifting of this protection by the applied magnetic field leads to the XMR, which is highly dependent on mobility in the topological materials [9]. Some of the XMR materials were also confirmed to be the topological semimetals, including Cd_3As_2, TaAs family, $PtSn_4$, and ZrSiS etc. [10–14]. The third is the open orbit condition [15,16]. In $PdCoO_2$, the motion of carriers along the open orbits was considered to be the explanation of its XMR property ($\mathrm{MR} \sim 10^5$%, $T = 2$ K, $B = 14$ T) according to the experimental and theoretical work by Takatsu and co-workers [17]. Besides, the open Fermi surface has also been observed in other XMR materials such as ZrSiS, $MoAs_2$, SiP_2, γ-$PtBi_2$, and WP_2 [18–23]. In these materials, the MR will rise in square with B remarkably when the magnetic field turns to the vertical direction of the Fermi surface with open orbits and the direction of the current is in the open orbits [15,16].

Transition-metal borides (TMBs) are prized refractory materials which have attracted a lot of attention for their high melting points, high hardness, and excellent electrical and thermal conductivities [24–31]. Besides these mechanical properties, fruitful electrical properties have also been found in the borides. A serious superconductors were found in the borides such as MgB_2, $R_ENi_2B_2C$ (R_E= rare earth elements), $R_EPd_2B_2C$, $R_EPt_2B_2C$, $La_3Ni_2B_2N_3$ and so on [31–37]. Lately, the binary borides TiB_2, ZrB_2, and HfB_2 were reported as the nodal-lines semimetals theoretically and experimentally. Extremely large magnetoresistance property were found in these materials [29,30,38,39].

Recently, a new family of ternary transition-metal borides, MAB phase was synthesized and characterized [27,28,40–43]. These compounds are structured with hard boride layers interleaved with Al layers. Among them, MoAlB is the only transition-metal boride that forms alumina over its surface to prevent further oxidation when heated in air up to 1400 °C and is thus potentially useful for high-temperature applications, which have attracted a lot of attention [27,28,41–43]. Besides, MoAlB possess good thermal conductivity ($\kappa = 35\ \mathrm{Wm^{-1}\,K^{-1}}$ at 26 °C), which makes it easer to transfer the heat out [27]. Additionally, election transport experimental results show a metallic behavior in the MoAlB polycrystal with the resistivity ranged from 0.36 to 0.49 $\mu\Omega$ m at room temperature [27], a typical value of a semimetal. However, experimental research on the electrical properties of the MoAlB single crystal is still scarce.

Here, we grew MoAlB single crystals and studied the electrical properties in it. We found that MoAlB single crystal shows a typical metallic behavior that the resistivity decreases as the temperature cooling down. In the magnetic field, MoAlB shows large quadratical magnetoresistance up

*zhaolx@hust.edu.cn
†zengwei.zhu@hust.edu.cn

to 1650% ($B = 14$ T) without trend of saturation. In order to further understand the large magnetoresistance and carriers property in MoAlB, we studied the Hall effect at 2 K and found the coexistence of electrons and holes with similar carrier densities and high carrier mobilities in MoAlB. Moreover, clear Shubnikov-de Haas (SdH) oscillations were observed in both magnetoresistivity and Hall resistivity. Through analyzing the quantum oscillations, we revealed that several relatively small Fermi pockets occupied in the Brillouin zone and small cyclotron masses in MoAlB. Furthermore, we measured the angle dependence of SdH oscillations and mapped out the topology of the Fermi surfaces. We discovered that the Fermi surfaces exhibit quasi-two-dimensional property in MoAlB. We found that the axis of the open orbits is along the b axis. So the open orbital does not contribute to the large MR because the magnetic field is not perpendicular to the plane containing the axis of the open orbits and the direction of the current is not in the open orbit either. We conclude that the large magnetoresistance property in MoAlB is attributed to the scenarios of the carriers compensation when the magnetic field parallel to b axis, where MR reached 1650% at $T = 2$ K and $B = 14$ T.

II. EXPERIMENT

MoAlB single crystals were grown by the flux method. Firstly, high purity powder of Mo (99.9%), Al (99.9999%), and B (99.9%) were weighed with the molar ratio Mo : B : Al = 1 : 1 : 50. The reactants were placed in an alumina crucible with a cap. The crucible was transferred into a tube furnace with the shielding gas Ar flow through. Then, the temperature was increased to 1500 °C, held for 10 hours, and cooled down to 800 °C with 1 °C per hour and the furnace was turned off. Subsequently, the alumina crucible was sealed in a evacuated quartz ampoule and reheated to 800 °C. After a quick centrifugation, the rodlike single crystals were separated from the flux. The obtained crystals were characterized by x-ray diffraction (XRD) recorded by a PANalytical diffractometer with Cu k_α radiation ($\lambda = 1.5406$ Å). The atomic proportion was determined by energy dispersive x-ray (EDX) spectroscopy. The transport measurements were performed on a physical property measurement system (Quantum Design PPMS-16) and a TeslatronPT (Oxford Instruments) equipped with a homemade rotator whose angle can be controlled by a data-collecting computer. The electrical current was applied by a Keithley 6221 and the voltage was measured by a Keithley 2182A.

III. RESULTS

The crystal structure of MoAlB was reported to be an orthorhombic system with the space group of *Cmcm*. The refined lattice parameters are $a = 3.2162$ Å, $b = 14.062$ Å, $c = 3.1030$ Å, $\alpha = \beta = \gamma = 90°$ [43]. Figure 1(a) shows the crystal structure of MoAlB, MoB sublattice, and Al bilayer stack along the b axis. Figure 1(b) shows the image of as-grown MoAlB single crystal with the size of $3.5 \times 0.8 \times 0.2$ mm^3. Figure 1(c) is the XRD pattern of the MoAlB single crystal. Only the set of (0 k 0) is observed, indicating the facet of the sample shown in the inset of Fig. 1(b) is the ac plane.

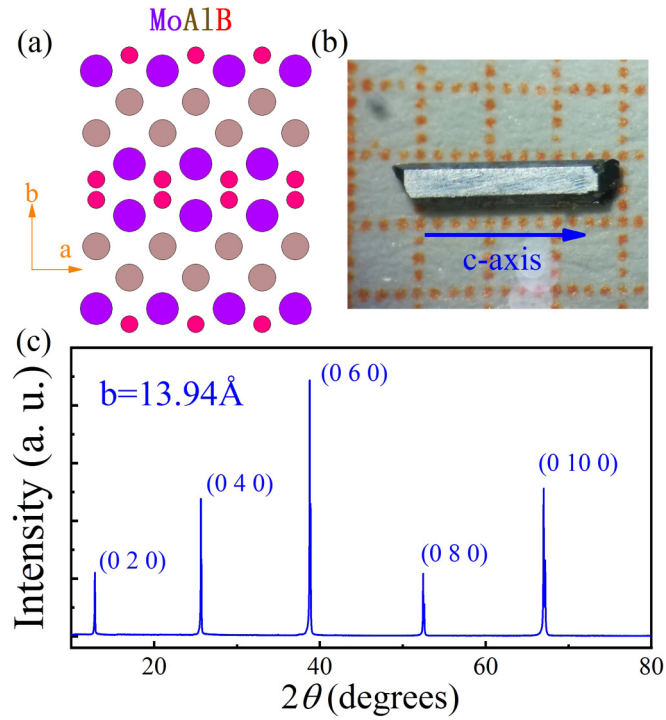

FIG. 1. (a) Crystal structure of MoAlB. (b) A photo of a MoAlB single crystal with the typical size of $3.5 \times 0.8 \times 0.2$ mm^3. (c) X-ray diffraction pattern of MoAlB single crystal, showing only the (0 k 0) reflection.

The lattice parameter $b = 13.94$ Å was calculated from our experiment, which is in agreement with the reported result. Additionally, we confirmed that the long edge of the sample is along the c axis, which was labeled with the blue arrow in the inset of Fig. 1(b). During all of our measurements, the current was kept along the c axis.

Figure 2(a) shows the temperature dependence of resistivity under various magnetic fields. At $B = 0$ T, MoAlB sample shows a typical metallic behavior with the residual resistivity ratio RRR = $\rho(300\text{ K})/\rho(1.8\text{ K}) = 40$. When the magnetic field beyond 9 T is applied, the resistivity shows a quick upturn behavior and saturates to a plateau as the temperature is cooling down. Similar behaviors have been observed in topological semimetals and compensated semimetals [1,4,11,13], which exhibit high carrier mobility at low temperatures. In order to further understand the carriers property in MoAlB, we measured magnetoresistivity and the Hall resistivity at 2 K [shown in Fig. 2(b)]. The MR increases quadratically with the magnetic field and finally approaches 1650 % at $T = 2$ K under the magnetic field of 14 T without any sign of saturation. Besides, the value of magnetoresistance in MoAlB is significantly larger than that in the typical metal such as Au, Ag, and Cu, although it cannot be comparable to those in the representative large magnetoresistance materials: WTe_2, $TaAs_2$, or TaAs [1,6,11]. The slope of the Hall resistivity changes with the magnetic field indicating a multiband property is dominated in the transport measurement. We found that the in-plane anisotropy in MoAlB is so small that the resistivity along a axis and c axis are nearly the same. (Shown in the Fig. S1 in the "Supplemental Material" [44].) So we

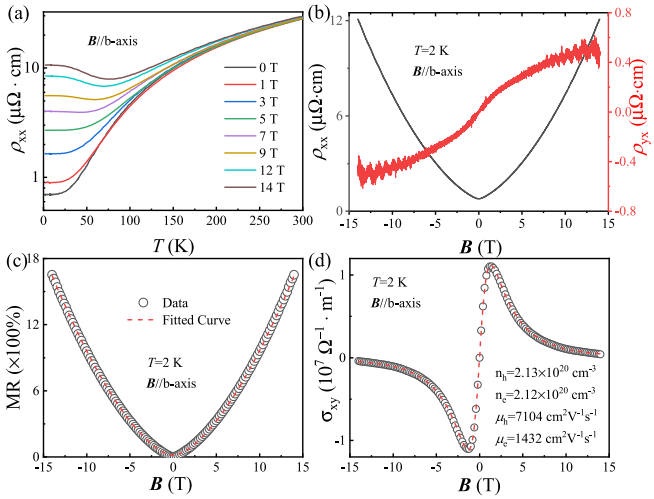

FIG. 2. (a) Temperature dependence of the resistivity under different magnetic fields ($B = 0$ T, 1 T, 3 T, 5 T, 7 T, 9 T, 12 T, and 14 T). (b) Magnetic field dependence of magnetoresistivity and Hall resistivity at 2 K as the magnetic field is perpendicular to the current. (c) The magnetic field dependence of MR (MR = $[(\rho(B)\text{-}\rho(0))/\rho(0)]\times 100\%$) at 2 K, which can be fitted by a quadratic function. The fit result was plotted with a red dashed line. (d) Magnetic field dependence of σ_{xy} at 2 K. The open cycles and the dashed line represent the measured data and the fitted result with the two-carrier model, respectively.

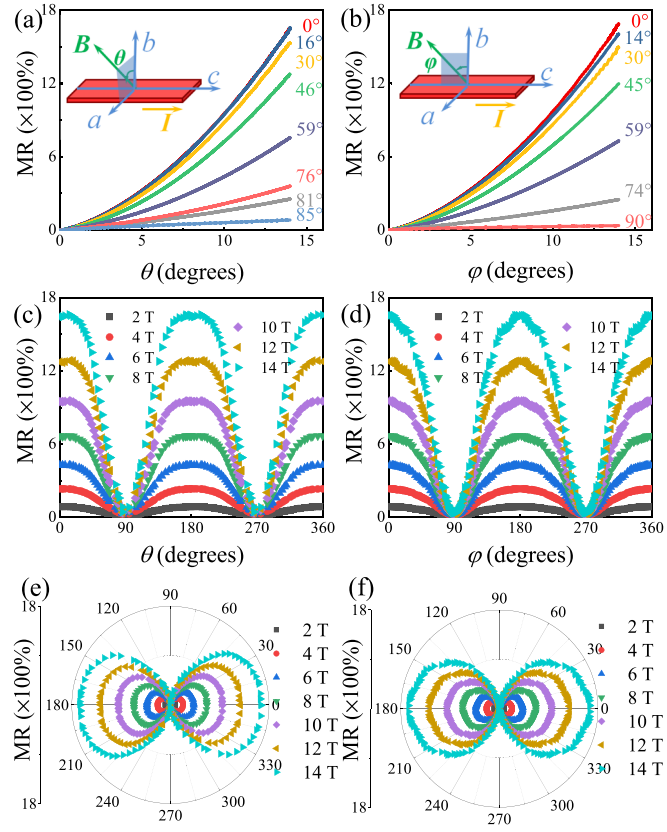

FIG. 3. (a), (b) MR of MoAlB at 2 K under magnetic fields applied at different angles θ and φ, respectively. The insets show the measurement configurations. (c), (d) The angle dependence of the MR under 2 K at different magnetic fields. (e), (f) The polar plot for the angle dependence of MR under 2 K at different magnetic fields, corresponding to (c) and (d), respectively.

fitted the carrier densities and mobilities by using the two-carrier model below.

$$\sigma_{xy}(B) = \frac{\rho_{yx}(B)}{\rho_{xx}^2(B) + \rho_{yx}^2(B)} = \left[\frac{n_h\mu_h^2}{1+(\mu_h B)^2} - \frac{n_e\mu_e^2}{1+(\mu_e B)^2}\right]eB \qquad (1)$$

Here, n_h (n_e) denotes the carrier density of holes (electrons) and μ_h (μ_e) denotes the mobility of holes (electrons), respectively. The fitted result is shown in Fig. 2(d), which yields carrier densities of $n_h = 2.13 \times 10^{20}$ cm^{-3} (hole) and $n_e = 2.12 \times 10^{20}$ cm^{-3} (electron) with corresponding carrier mobilities of $\mu_h = 7104$ cm^2 V^{-1} s^{-1} (hole) and $\mu_e = 1432$ cm^2 V^{-1} s^{-1} (electron). The scale of the carriers density indicates that MoAlB is a typical semimetal and the carriers compensation with high mobility in MoAlB should be one of the reasons which cause the large unsaturated quadratic MR.

To investigate the anisotropy of MoAlB, we measured the angle dependence of the ρ_{xx} by rotating the sample around its c axis (θ) and a axis (ϕ) separately shown in Figs. 3(a) and 3(b). During the measurements, the current was applied along the c axis [the blue arrow in Fig. 1(b)]. The measurement configurations are shown in the inset of Figs. 3(a) and 3(b). The MR raises quadratically with the magnetic field increasing but decreases gradually when tilting the magnetic field from $\theta = 0^\circ$ to $\theta = 90^\circ$ at the same fields. Figure 3(c) shows MR at 2 K and under magnetic fields of 2 T, 4 T, 6 T, 8 T, 10 T, 12 T, and 14 T, with tilting the magnetic field around the c axis. Results were also plotted with a polar plot shown in Fig. 3(e). Under 14 T, the amplitude of MR decreases from 1650% to 80% as the angle θ is increased from 0° to 90° when the current is applied along the c axis. The anisotropy of the magnetoresistance (MR(θ=0°)/MR(θ=90°)) is up to 2060% under this circumstance, which reflect the anisotropy of the carrier mobility on the Fermi surface. We also carried out the similar MR measurements by tilting the magnetic field around the a axis, shown in Fig. 3(b), Fig. 3(d), and Fig. 3(f). The MR decreases from 1650% to 36% as the angle φ is increased from 0° to 90°, and the anisotropy of the magnetoresistance (MR(φ=0°)/MR(φ=90°)) is up to 4600%. Under this circumstance, the component of the magnetic field perpendicular to the current decreases when the angle φ is increasing, which further enlarge the anisotropy of the magnetoresistance in the bc plane.

During our measurements, evident SdH oscillations were observed under low temperatures. We studied the quantum oscillations carefully. Figure 4 shows the SdH oscillations extracted from the ρ_{xx} when the magnetic field is parallel to the b axis. Figure 4(a) presents the oscillatory parts against the reciprocal of the magnetic field $1/B$. Figure 4(b) presents the fast Fourier transformation (FFT) spectrum of $\Delta\rho_{xx}$ at different temperatures. Four fundamental frequencies can be identified clearly which are labeled as F_α (134.4 T), F_β (229.5 T), F_γ (946.2 T), and F_δ (1080.5 T). According to the Onsager relation, $F = (\hbar c/2\pi e)A_k$, the oscillation

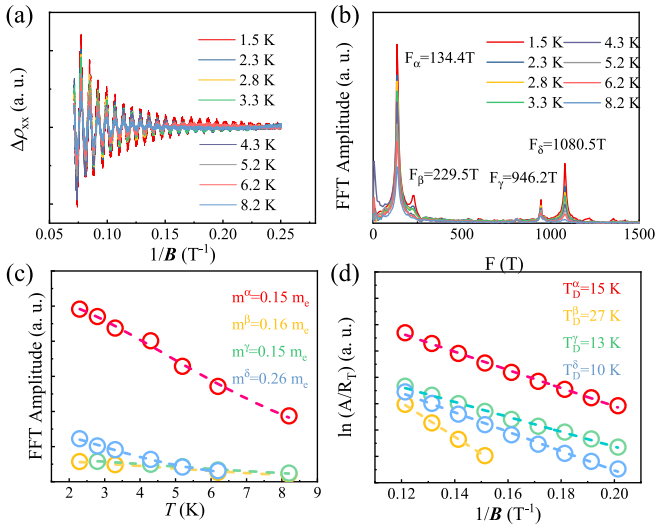

FIG. 4. SdH oscillations of MoAlB. (a) The oscillatory part of ρ_{xx} of MoAlB with B $\parallel$ b axis at different temperatures. (b) The FFT spectrum of $\Delta\rho_{xx}$ at different temperatures. Four frequencies are extracted. (c) Temperature dependence of the amplitude for the four frequencies, and the dashed curves are theoretical fittings to the Lifshitz-Kosevich formula. (d) Dingle temperatures of the different pockets.

frequency is proportional to the extreme cross section. We calculated the extremal Fermi surface area, which are $S_F^\alpha = 0.013$ Å^{-2}, $S_F^\beta = 0.022$ Å^{-2}, $S_F^\gamma = 0.090$ Å^{-2}, and $S_F^\delta = 0.103$ Å^{-2} occupying 0.32%, 0.55%, 2.3%, and 2.6% of the $k_a k_c$ plane of the Brillouin zone, respectively. As temperature increased, the oscillatory amplitude damps out gradually with the temperature increasing. The amplitude can be expressed by the Lifshitz-Kosevich formula [5]: $R_T = \frac{X}{\sinh X}$ and impurity scattering $R_D = \exp(-\frac{\pi m^*}{eB\tau_Q})$ where $X = \frac{2\pi^2 k_B T m^*}{e\hbar B}$, m^* is the cyclotron mass, and T_D is the Dingle temperature. We plot the temperature dependence of the amplitude and the fitted curves for these frequencies in Fig. 4(c). The fitted cyclotron mass are $m_\alpha^* = (0.15 \pm 0.03)m_e$, $m_\beta^* = (0.16 \pm 0.02)m_e$, $m_\gamma^* = (0.15 \pm 0.01)m_e$, and $m_\delta^* = (0.26 \pm 0.07)m_e$, which are much lighter than the mass of the free electron. The obtained Dingle temperatures are $T_D^\alpha = 15$ K, $T_D^\beta = 27$ K, $T_D^\gamma = 13$ K, and $T_D^\delta = 10$ K for α, β, γ, and δ bands, respectively. Quantum scattering lifetime τ_Q is reciprocal to the Dingle temperature: $\tau_Q = \hbar/2\pi k_B T_D$. In the current sample, $\tau_Q^\alpha = 8.1 \times 10^{-14}$ s, $\tau_Q^\beta = 4.5 \times 10^{-14}$ s, $\tau_Q^\gamma = 9.4 \times 10^{-14}$ s, and $\tau_Q^\delta = 1.2 \times 10^{-13}$ s. The quantum mobilities are estimated by $\mu_Q = (e\tau_Q/m^*)$, yielding $\mu_Q^\alpha = 950$ cm^2 V^{-1} s^{-1}, $\mu_Q^\beta = 494$ cm^2 V^{-1} s^{-1}, $\mu_Q^\gamma = 1095$ cm^2 V^{-1} s^{-1}, and $\mu_Q^\delta = 821$ cm^2 V^{-1} s^{-1}, which are about one order lower than μ_{tr}. The transport lifetime $\tau_{tr} = \mu m^*/e$ is about 10^{-12} s. The large ratio of τ_{tr}/τ_Q and μ_{tr}/μ_Q suggests that the small angle scattering is dominant in MoAlB [45,46]. We listed results in the Table I. Additionally, we found several other FFT frequencies with relatively small amplitude which were shown in Fig. S2 in the "Supplemental Material" [44]. These frequencies were further confirmed through the angle dependent spectrum discussed below.

In the previous work, M. A. Ali *et al.* [47] calculated the band structure of MoAlB and mapped the Fermi surface by using the first principle calculation. They pointed out that there exist nearly two-dimensional Fermi surface structure in MoAlB. However, there is no experimental study of the Fermi surface in MoAlB before. Quantum oscillation measurement is an effective method to calibrate the Fermi surface in metals. We studied angle dependence of SdH on the magnetoresistance as we rotated the sample around the c axis and the a axis. The schematic diagrams of experimental setups are the same as shown in the inset of Fig. 3(a) and Fig. 3(b). We obtain the FFT spectra evolving with the angle as the magnetic field is titling from (010) to (100) and (010) to (001) separately, shown in Fig. 5(a) and Fig. 5(b). As seen in Fig. 5(a), most of the frequencies increase obviously and the become indistinguishable as the angle θ is increased from 0° to 90°, except the band F_α' emerges around 60°. Besides, the nearly indistinguishable frequency F_χ turns clear with the angle θ increasing. In order to clarify the symmetry of the Fermi surface, we plotted the angle dependence of fundamental frequencies in a polar plot in Fig. 5(c). The drumlike, pulvinate, and cylindrical extremal orbits exists in the $k_a k_b$ plane, indicating high anisotropy in this plane. Figure 5(b) shows the angular dependence of the extremal orbits from (010) to (001). Similarly, we plotted it in a polar plot. In Fig. 5(d), most of the Fermi surfaces show obvious anisotropy, except the band F_χ which is in an ellipselike shape.

Open orbit is another possible reason which may cause large MR in semimetals/metals when the direction of the magnetic field turns to the vertical direction of the Fermi

TABLE I. Summary of the physical properties for the four pockets in the $k_a k_c$ plane: frequencies (F), external Fermi surface area (S_F), cyclotron mass (m^*), Dingle temperature (T_D), relaxation time (τ_Q), and quantum mobilities (μ_Q) of each pockets when the magnetic field is paralleled to the b axis.

Pockets	α	β	γ	δ
F (T)	134.4	229.5	946.2	1080.5
S_F (Å^{-2})	0.013	0.022	0.090	0.103
Fraction	0.32%	0.55%	2.3%	2.6%
m^* (m_e)	0.15 ± 0.03	0.16 ± 0.02	0.15 ± 0.01	0.26 ± 0.07
T_D (K)	15	27	13	10
τ_Q (s)	8.1×10^{-14}	4.5×10^{-14}	9.5×10^{-14}	1.2×10^{-13}
μ_Q (cm^2/Vs)	950	495	1095	822

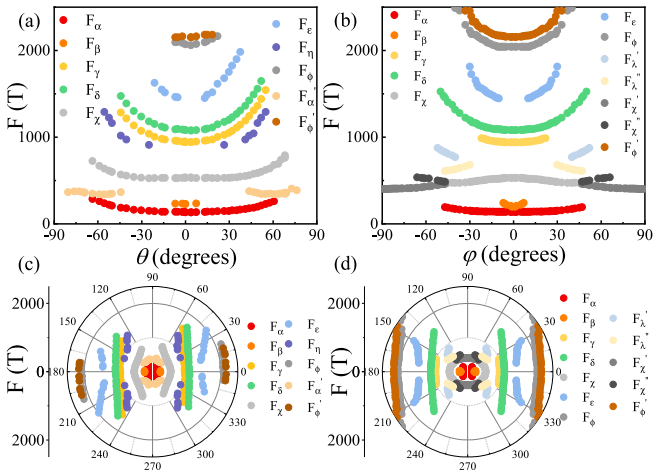

FIG. 5. Angle dependence of the SdH oscillations of MoAlB. (a),(b) FFT spectra of SdH oscillations as a function of frequencies when the angle θ (φ) from -90° to 90°. (c),(d) The polar plot for the angle dependence of the SdH frequencies. The circles are for experimental data from the peaks of the FFT spectra.

surface with open orbits and the direction of the current is in the open orbits [15,16]. In MoAlB, we discovered the columnar like quasi-two-dimensional Fermi surfaces with the open axis along the *b* axis. In our measurement, the maximum MR emerged when the magnetic parallel to the *b* axis where the open orbit does not work on large MR. We conclude that it's the carrier compensation with high carrier mobility cause the large MR (1650%) when the magnetic field is applied along the *b* axis in MoAlB. Searching more XMR materials with two-dimensional property is in need to further understand the large MR caused by the open orbit mechanism.

IV. CONCLUSION

In summary, we grew high quality MoAlB single crystals and observed a large magnetoresistance in it. MR approaches 1650% at 2 K, 14 T without saturation. The analysis of Hall effect points out that the carriers compensation scenario is one of the possible reasons which causes the large magnetoresistance property in MoAlB. Clear SdH oscillations have been observed and several fundamental frequencies can be clearly identified. We extracted cyclotron mass, Dingle temperature, relaxation time, and carriers mobilities through SdH oscillations, which suggest the small angle scattering is dominant in MoAlB. Besides, we observed significant anisotropy of MR in the $k_a k_b$ and $k_b k_c$ planes, indicating an anisotropic electronic structure in MoAlB. The angle dependence of SdH oscillations illustrate that there exists quasi-two-dimensional Fermi surfaces which can induce significant anisotropy of both FFT frequencies and MR in MoAlB.

ACKNOWLEDGMENTS

This work was supported by the National Key Research and Development Program of China (Grant No. 2016YFA0401704), the National Science Foundation of China (Grants No. 51861135104 and No. 11574097), the Fundamental Research Funds for the Central Universities (Grant No. 2019kfyXMBZ071), and the China Postdoctoral Science Foundation (Grant No. 2018M630846).

[1] M. N. Ali, J. Xiong, S. Flynn, J. Tao, Q. D. Gibson, L. M. Schoop, T. Liang, N. Haldolaarachchige, M. Hirschberger, N. P. Ong, and R. J. Cava, Nature (London) **514**, 205 (2014).
[2] Z. Zhu, X. Lin, J. Liu, B. Fauqué, Q. Tao, C. Yang, Y. Shi, and K. Behnia, Phys. Rev. Lett. **114**, 176601 (2015).
[3] L. X. Zhao, Q. N. Xu, X. M. Wang, J. B. He, J. Li, H. X. Yang, Y. J. Long, D. Chen, H. Liang, C. H. Li, M. Q. Xue, J. Q. Li, Z. Ren, L. Lu, H. M. Weng, Z. Fang, X. Dai, and G. F. Chen, Phys. Rev. B **95**, 115119 (2017).
[4] W. S. Gao, N. N. Hao, F. W. Zheng, W. Ning, M. Wu, X. D. Zhu, G. L. Zheng, J. L. Zhang, J. W. Lu, H. W. Zhang, C. Y. Xi, J. Y. Yang, H. F. Du, P. Zhang, Y. H. Zhang, and M. L. Tian, Phys. Rev. Lett. **118**, 256601 (2017).
[5] L. X. Zhao, L. C. Xu, H. K. Zuo, X. M. Wu, G. Y. Gao, and Z. W. Zhu, Phys. Rev. B **98**, 085137 (2018).
[6] Y.-Y. Wang, Q.-H. Yu, P.-J. Guo, K. Liu, and T.-L. Xia, Phys. Rev. B **94**, 041103(R) (2016).
[7] K. F. Wang, D. Graf, L. J. Li, L. M. Wang, and C. Petrovic, Sci. Rep. **4**, 7328 (2014).
[8] J. Xu, N. J. Ghimire, J. S. Jiang, Z. L. Xiao, A. S. Botana, Y. L. Wang, Y. Hao, J. E. Pearson, and W. K. Kwok, Phys. Rev. B **96**, 075159 (2017).
[9] S. Singh, V. Süß, M. Schmidt, C. Felser, and C. Shekhar, J. Phys.: Materials **3**, 024003 (2020).
[10] T. Liang, Q. Gibson, M. N. Ali, M. Liu, R. J. Cava, and N. P. Ong, Nat. Mater. **14**, 280 (2014).
[11] X. C. Huang, L. X. Zhao, Y. J. Long, P. P. Wang, D. Chen, Z. H. Yang, H. Liang, M. Q. Xue, H. M. Weng, Z. Fang, X. Dai, and G. F. Chen, Phys. Rev. X **5**, 031023 (2015).
[12] C. Shekhar, A. K. Nayak, Y. Sun, M. Schmidt, M. Nicklas, I. Leermakers, U. Zeitler, Y. Skourski, J. Wosnitza, Z. Liu, Y. Chen, W. Schnelle, H. Borrmann, Y. Grin, C. Felser, and B. Yan, Nat. Phys. **11**, 645 (2015).
[13] N. H. Jo, Y. Wu, L. L. Wang, P. P. Orth, S. S. Downing, S. Manni, D. Mou, D. D. Johnson, A. Kaminski, S. L. Bud'ko, and P. C. Canfield, Phys. Rev. B **96**, 165145 (2017).
[14] G. Peramaiyan, R. Sankar, I. P. Muthuselvam, and W. L. Lee, Sci. Rep. **8**, 6414 (2018).
[15] S. N. Zhang, Q. S. Wu, Yi Liu, and Oleg V. Yazyev, Phys. Rev. B **99**, 035142 (2019).
[16] A. B. Pippard, *Magnetoresistance in Metals* (Cambridge University Press, New York, 1989).
[17] H. Takatsu, J. J. Ishikawa, S. Yonezawa, H. Yoshino, T. Shishidou, T. Oguchi, K. Murata, and Y. Maeno, Phys. Rev. Lett. **111**, 056601 (2013).
[18] Y. Y. Lv, B. B. Zhang, X. Li, S. H. Yao, Y. B. Chen, J. Zhou, S. T Zhang, M. H. Lu, and Y. F. Chen, Appl. Phys. Lett. **108**, 244101 (2016).

[19] R. Lou, Y. F. Xu, L.-X. Zhao, Z.-Q. Han, P.-J. Guo, M. Li, J.-C. Wang, B.-B. Fu, Z.-H. Liu, Y.-B. Huang, P. Richard, T. Qian, K. Liu, G.-F. Chen, H. M. Weng, H. Ding, and S.-C. Wang, Phys. Rev. B **96**, 241106(R) (2017).

[20] Y. Zhou, Z. Lou, S. N. Zhang, H. Chen, Q. Chen, B. Xu, J. Du, J. Yang, H. Wang, Q. S. Wu, O. V. Yazyev, and M. Fang, arXiv:2002.05258.

[21] B. Wu, V. Barrena, H. Suderow, and I. Guillamón, Phys. Rev. Res. **2**, 022042(R) (2020).

[22] N. Kumar, Y. Sun, N. Xu, K. Manna, M. Yao, V. Süss, I. Leermakers, O. Young, T. Förster, M. Schmidt, H. Borrmann, B. Yan, U. Zeitler, M. Shi, C. Felser, and C. Shekhar, Nat. Commun. **8**, 1642 (2017).

[23] J. Du, Z. Lou, S. N. Zhang, Y. Zhou, B. Xu, Q. Chen, Y. Tang, S. Chen, H. Chen, Q. Zhu, H. Wang, J. Yang, Q. Wu, Oleg V. Yazyev, and M. Fang, Phys. Rev. B **97**, 245101 (2018).

[24] H. Kim and D. R. Trinkle, Phys. Rev. Materials **1**, 013601 (2017).

[25] R. Lortz, Y. Wang, S. Abe, C. Meingast, Yu. B. Paderno, V. Filippov, and A. Junod, Phys. Rev. B **72**, 024547 (2005).

[26] D. Groh, W. J. Slough, R. Pandey, S. P. Karna, and D. Dandekar, Phys. Rev. B **83**, 115122 (2011).

[27] S. Kota, E. Z. Solvas, A. Ly, J. Lu, O. Elkassabany, A. Huon, W. E. Lee, L. Hultman, S. J. May, and M. W. Barsoum, Sci. Rep. **6**, 26475 (2016).

[28] S. Kota, M. Agne, E. Z.-Solvas, O. Dezellus, D. Lopez, B. Gardiola, M. Radovic, and M. W. Barsoum, Phys. Rev. B **95**, 144108 (2017).

[29] X. Feng, C. Yue, Z. Song, Q. S. Wu, and B. Wen, Phys. Rev. Materials **2**, 014202 (2018).

[30] Q. Wang, P. J. Guo, S. Sun, C. Li, K. Liu, Z. Y. Lu, and H. Lei, Phys. Rev. B **97**, 205105 (2018).

[31] J. Nagamatsu, N. Nakagawa, T. Muranaka, Y. Zenitani, and J. Akimitsu, Nature (London) **410**, 63 (2001).

[32] E. Johnston-Halperin, J. Fiedler, D. E. Farrell, Ming Xu, B. K. Cho, P. C. Canfield, D. K. Finnemore, and D. C. Johnston, Phys. Rev. B **51**, 12852 (1995).

[33] Warren E. Pickett and David J. Singh, Phys. Rev. Lett. **72**, 3702 (1994).

[34] X. Lu, W. K. Park, S. Yeo, K.-H. Oh, S.-I. Lee, S. L. Bud'ko, P. C. Canfield, and L. H. Greene, Phys. Rev. B **83**, 104519 (2011).

[35] G. Ghosh, A. D. Chinchure, R. Nagarajan, C. Godart, and L. C. Gupta, Phys. Rev. B **63**, 212505 (2001).

[36] S. K. Dhar, A. D. Chinchure, R. Nagarajan, S. M. Pattalwar, L. C. Gupta, E. Alleno, and C. Godart, Phys. Rev. B **65**, 132519 (2002).

[37] H. W. Zandbergen, J. Jansen, R. J. Cavai, J. J. Krajewskii, and W. F. Peck Jr, Nature (London) **372**, 759 (1994).

[38] Z. Liu, R. Lou, P. Guo, Q. Wang, S. Sun, C. Li, S. Thirupathaiah, A. Fedorov, D. Shen, K. Liu, H. Lei, and S. Wang, Phys. Rev. X **8**, 031044 (2018).

[39] C. J. Yi, B. Q. Lv, Q. S. Wu, B.-B. Fu, X. Gao, M. Yang, X.-L. Peng, M. Li, Y.-B. Huang, P. Richard, M. Shi, G. Li, Oleg V. Yazyev, Y. G. Shi, T. Qian, and H. Ding, Phys. Rev. B **97**, 201107(R) (2018).

[40] J. Lu, S. Kota, M. W. Barsoum, and L. Hultman, Mater. Res. Lett. **5**, 235 (2017).

[41] L. T. Alameda, P. Moradifar, Z. P. Metzger, N. Alem, and R. E. Schaak, J. Am. Chem. Soc. **140**, 8833 (2018).

[42] L. Xua, O. Shia, C. Liua, D. Zhua, S. Grassoa, and C. Hu, Ceramics International **44**, 13396 (2018).

[43] F. Z. Dai, Z. H. Feng, and Y. C. Zhou, Comp. Mater. Sci. **147**, 331 (2018).

[44] See Supplemental Material at http://link.aps.org/supplemental/10.1103/PhysRevB.102.075139 for anisotropic resistivity and detailed FFT spectrum from 0 to 2500 T.

[45] A. Narayanan, M. D. Watson, S. F. Blake, N. Bruyant, L. Drigo, Y. L. Chen, D. Prabhakaran, B. Yan, C. Felser, T. Kong, P. C. Canfield, and A. I. Coldea, Phys. Rev. Lett. **114**, 117201 (2015).

[46] R. Kealhofer, S. Jang, S. M. Griffin, C. John, K. A. Benavides, S. Doyle, T. Helm, P. J. W. Moll, J. B. Neaton, J. Y. Chan, J. D. Denlinger, and J. G. Analytis, Phys. Rev. B **97**, 045109 (2018).

[47] M. A. Ali, M. A. Hadi, M. M. Hossain, S. H. Naqib, and A. K. M. A. Islam, Phys. Status. Solidi. B **254**, 1700010 (2017).